energies

MDPI

Article

Power Performance Analysis Based on Savonius Wind Turbine Blade Design and Layout Optimization through Rotor Wake Flow Analysis

Heejeon Im [1] and Bumsuk Kim [2,*]

[1] Multidisciplinary Graduate School Program for Wind Energy, Jeju National University, Jeju 63243, Republic of Korea
[2] Faculty of Wind Energy Engineering, Graduate School, Jeju National University, Jeju 63243, Republic of Korea
* Correspondence: bkim@jejunu.ac.kr

Abstract: Savonius vertical axis wind turbines have simple structures, can self-start in environments with low wind speed and strong turbulence intensity, and can be installed at low costs. Therefore, installation is possible in urban centers with low wind speeds, which may contribute to the construction of a decentralized power system. Savonius wind turbines are operated by drag force, with the blades moving in the same direction as the flow current providing the thrust force and those moving in the opposite direction of the wind being rotated by the drag force. In this study, the Savonius wind turbine design was examined to develop a stable wind turbine for use in urban centers at low wind speeds. The Savonius rotor design variables (aspect and overlap ratios) and blade forms (semi-circular, Bach, and elliptical type) were examined using computational fluid dynamics analysis. Moreover, a rotor capable of providing the target output was designed and maximum rotor efficiency of 18% was realized. Further, changes to the flow corresponding with various turbine layouts were analyzed to determine the arrangement that would maximize turbine performance. The results showed that the maximum efficiency of the turbines was in the 17–19% range and without significant variation.

Keywords: numerical simulation; vertical axis wind turbine; savonius rotor; wake; layout

Citation: Im, H.; Kim, B. Power Performance Analysis Based on Savonius Wind Turbine Blade Design and Layout Optimization through Rotor Wake Flow Analysis. *Energies* **2022**, *15*, 9500. https://doi.org/10.3390/en15249500

Received: 31 October 2022
Accepted: 12 December 2022
Published: 14 December 2022

1. Introduction

Global cumulative wind power capacity grew rapidly to 778 GW in 2020, and is expected to reach 1247 GW in 2025. This translates to an annual average growth rate of 8.4% in comparison to 2020 [1]. In modern large-scale wind farms, horizontal axis wind turbines with high efficiency are used. Currently, the global wind power market is focused on the development of the offshore wind power industry because the onshore wind power market has reached saturation level and is subject to the imposition of restrictions on new installations arising out of environmental concerns. However, offshore wind turbine installations pose unique challenges compared to onshore wind turbines, owing to water depth as well as the higher installation and maintenance costs. Therefore, it is necessary for each country to expand the use of small wind turbines to increase the proportion of renewable energy generated and thereby achieve energy independence. The dissemination of small wind turbines along with photovoltaic systems has the potential to increase the energy self-sufficiency rate and contribute to the development of a decentralized power system. Among the small wind turbines, vertical axis wind turbines with relatively low rotational speeds provide greater structural stability than horizontal axis wind turbines, which generally operate at high rotational speeds [2]. Further, vertical axis wind turbines are more favorable from a maintenance standpoint because they do not require yaw movement controls and the main machinery is installed closer to the ground.

Among vertical axis wind turbines, Savonius wind turbines have lower noise and wear and tear of parts owing to lower rotational speeds [3]. Because they are not affected by the wind direction and require simpler support structures, their manufacturing costs are also lower [4]. However, because Savonius wind turbines exhibit lower efficiencies than Darrieus turbines, studies to improve their overall performance have been conducted. Particularly, research on the benefits of applying additional devices, such as nozzles [5], V-shaped wedge deflectors [6], deflecting plates [7], curtains [8], venting slots [9], and guide vanes [10] has been conducted. However, it is worth noting that the efficiency of Savonius wind turbines does not exceed the 20 to 30% range even with the application of aforementioned additional devices [11]. The application of these additional devices had the negative effect of countering the inherent benefits of Savonius wind turbines by increasing their manufacturing cost and decreasing their structural stability. Consequently, many researchers have conducted studies to improve the turbine performance by changing the blade geometry and other design parameters.

Among the design parameters of Savonius turbine blades, those that have the largest effects on performance are the aspect ratio (AR) and overlap ratio (OR). The AR is defined as the ratio between the rotor height and rotor diameter; the AR and angular velocity increase as the rotor height increases and diameter decreases [12]. Akwa [2] analyzed the flow characteristics of the Savonius rotor through an experimental study, and the results revealed an effect similar to that of the endplate in correspondence with the AR. Although increase in AR improves rotor performance, increase in rotor height results in structural instability; thus, there is a limit to how far the AR can be increased. Moreover, the efficiency does not significantly increase beyond a certain value even when the AR is increased [13]. The ratio of the blade width and blade overlap length is defined as the OR. The blade length varies in correspondence to the OR because each blade is overlapped, even for the same rotor diameter. However, when the overlap area between the blades is increased by increasing the OR, the rotor performance decreases owing to the expansion of the recirculated flow [14]. Therefore, several experimental and numerical analysis studies have been conducted to determine the OR that leads to the best turbine performance. Through an experimental study, Blackwell et al. [15] found that turbine performance reached its peak when the OR was between 0.1 and 0.15. Ushiyama [16] reported that maximum efficiency could be attained in a Savonius rotor with an OR of 0.167. Furthermore, based on numerical analysis, Akwaet et al. [17] stated that the highest turbine efficiency was attained when the AR is 0.15, whereas Gupta et al. [18] observed the highest efficiency at AR value of 0.2. Even though these research results establish that turbine performance is influenced by the AR and OR of the Savonius rotor, accurate AR and OR values have not yet been determined.

To determine a Savonius rotor design that is suitable for meeting the objectives, each design parameter must be re-examined. A blade geometry with a semi-circular bucket structure was used during the early development stages of the Savonius turbine. Subsequently, several studies have been conducted to determine a blade geometry that can improve the turbine efficiency aerodynamically. For instance, Ushiyama et al. [19] compared the efficiency of the semi-circular and the Bach rotors through numerical analysis and reported that the Bach rotors had superior performance. Similarly, Banerjee et al. [20] compared the performance of the semi-circular and elliptical rotors through numerical analysis and found that the elliptical type achieved superior performance. Alom et al. [21] compared the wind tunnel test results and numerical analysis results for semi-circular, Benesh, Bach, and elliptical Savonius rotors. They reported that the elliptical type had the highest rotor efficiency. The numerical analysis in the above study was conducted using two-dimensional (2D) unsteady simulations without considering flow in the rotor height direction, and the efficiency determined was higher than that obtained in the wind tunnel test results. As mentioned previously, the main design parameters of Savonius rotors are the AR and OR, which significantly influence the rotor performance. Therefore, three-dimensional (3D) unsteady simulation is required because it is necessary to analyze the effects of the spaces between the blades on the flow.

In this study, the Savonius turbine that has the capability to generate power even in low wind speed areas owing to its lower rotor operating speed has been utilized as the reference geometry to develop user-friendly urban wind turbines. The objectives were to ensure the stability of the rotor blade in unexpected situations and develop an eco-friendly turbine using recycled fabric materials such as discarded banners. Because recycled fabric materials were used, a complex blade geometry such as a twisted blade could not be adopted. Therefore, among various Savonius rotor types it became necessary to determine the rotor geometry that would enable stable power generation while taking manufacturability into consideration. Consequently, the simple semi-circular type was determined as the most suitable geometry in this study, and its performance was compared to that of the Bach and elliptical types. The main design parameters, that is to say, the AR and OR, of the semi-circular type were determined through 3D unsteady simulation analysis, and the change in rotor performance in correspondence with the design parameters of the Bach and elliptical types was analyzed. Savonius wind turbines exhibit a significant difference in power generated depending on the rotational position of the rotor. Therefore, the rotor geometry with the lowest difference between minimum and maximum power generated according to the rotational position of the rotor was chosen as the final geometry. Furthermore, because of the necessity to install a large number of wind turbines in a narrow space in the case of small wind turbines, a rotor arrangement that factors in the influence of the wake was adopted. The rotor rotation direction and rotor spacing that minimizes the interference between the turbines when a large number of wind turbines are installed were examined. The flow characteristics of each rotor were analyzed according to its rotational position. After arranging up to three rotors, the performance change of each rotor was analyzed and the optimal position of each rotor was suggested based on the findings.

2. Numerical Method

For wind turbine design, it is necessary to examine the turbine's performance under various operating conditions. Because experimental research involving wind tunnel tests requires considerable time and cost, numerical analysis is conducted in the initial design stage. For vertical axis wind turbines such as Savonius wind turbines, 3D transient flow analysis is required because the torque significantly varies depending on the rotational position of the rotor. In this study, Simcenter STAR-CCM+V15.04 (Siemens) commercial software was used, and the k-ω shear stress transport (SST) gamma re-theta turbulence model based on Reynolds-averaged Navier–Stokes (RANS) equations was applied to analyze the effects of flow and wake in the area in which the blades are overlapped. The time step was set to the rotation interval of 1° of the rotor and was calculated based on the inlet wind speed and tip speed ratio. After the simulation started, when the rotor rotated once, the flow field was stabilized, and it was confirmed that the monitoring values converged in the same pattern from the second rotation. The total simulation time was set to five revolutions of the rotor. The average power of the rotor in the analysis result was calculated by averaging the power generated during the fifth rotation.

2.1. Boundary Condition and Grid Independence Test

The computational fluid dynamics (CFD) simulations performed in this study can be classified as single- and multiple-rotor simulations. The analysis model and boundary conditions of the single rotor are shown in Figure 1. For multiple rotors, the rotors and a rotating area were added considering the same conditions as those for the single rotor. For the rotating area of the Savonius rotor, a rectangular parallelepiped control volume with distances of 10D (where D is the rotor diameter) to the velocity inlet, 30D to the pressure outlet, and 5D to the top, bottom, and side surfaces from the rotor center was constructed under a velocity inlet whose flow direction was along the x axis, so that there was no effect from the flow analysis domain.

As the analysis model had a high curvature and the area in which the blades overlapped was small, the analysis results might vary depending on the grid system configura-

tion. The analysis model for the grid independence test had D = 0.8 m and a rotor height (H) of 1.28 m. The detailed design specifications are provided in Section 3. Because the RANS-based k-ω SST model was sensitive to the grid distance from the wall, the value of y+, which is the dimensionless wall distance, is important. Because the Savonius wind turbine was rotated by lift and drag, it was necessary to accurately simulate the velocity gradient inside the blade surface boundary layer. Therefore, the prism grid diffusion ratio was uniformly adjusted to 1.5 times by applying 20 prism grids in the viscous sub-layer area, and the grids were constructed so that the condition of y+ = 1 could be satisfied.

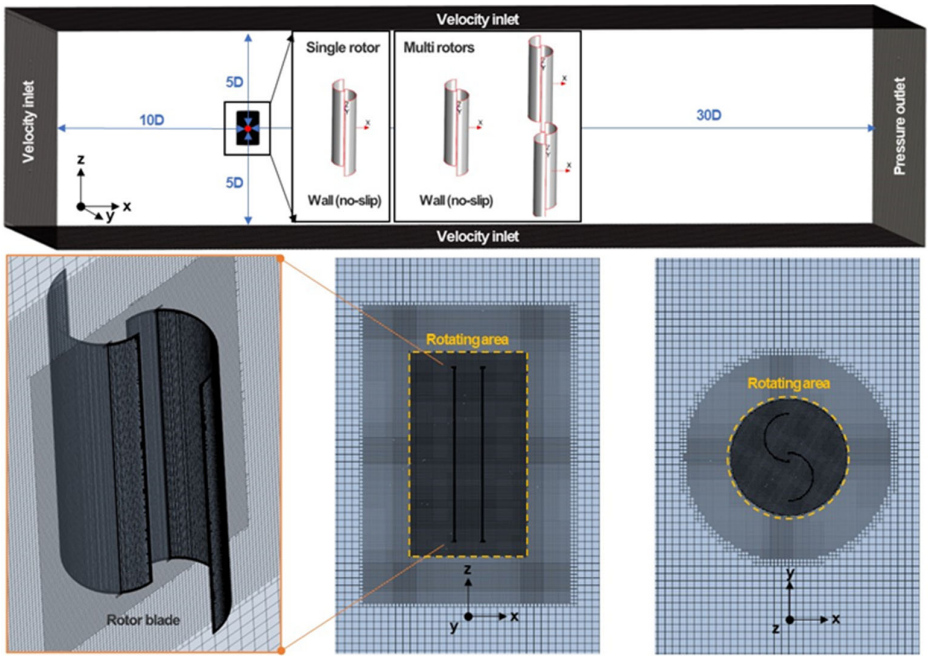

Figure 1. Boundary conditions and model for CFD analysis.

The trim mesh was constructed using the Simcenter STAR-CCM+ software as shown in Figure 1. The converging flow field and analysis model grids were examined. The resolution of the mesh under analysis was adjusted by the target size of the blade surface. The target sizes of the low-resolution, medium-resolution, and high-resolution meshes were 1.5×10^{-2}, 0.5×10^{-2}, and 0.1×10^{-2} m, respectively, and their total number of grids were 1.0×10^{7}, 1.6×10^{7}, and 3.0×10^{7}, respectively. As shown in Figure 2, the average power change in 1 s was similar for all resolutions. However, the power at low resolution exhibited a difference of more than 10% from that at high resolution. Moreover, because rotor speed increases with an increase in tip speed ratio (TSR), convergence may not occur and incorrect results may be obtained when the grid resolution is low. Therefore, in this study, analysis was conducted based on the grid level of 1.6×10^{7} cells, which does not significantly affect convergence despite increase in the rotor speed.

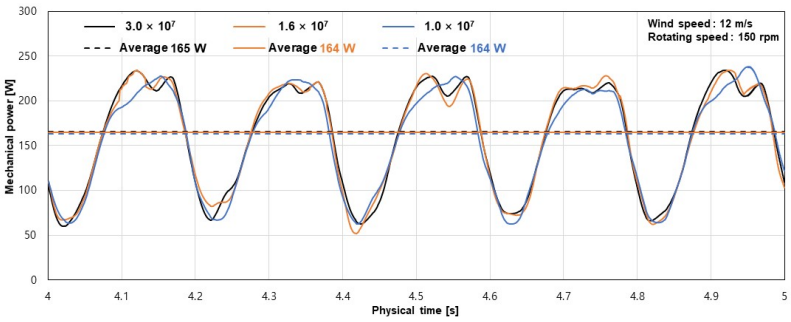

Figure 2. Rotor power according to number of grid cells.

2.2. Numerical Method Validation

To confirm the validity of the numerical analysis results, it was necessary to compare them with test data. As the research in this study was focused on the initial design stage, test data could be secured upon completion of the basic design. Therefore, the experimental data from previous studies [15,22] were used, and CFD analysis was conducted under the same conditions. The efficiency of the rotor was then compared according to the TSR change. The reference length for calculating the Reynolds number was based on a blade width of 0.45 m. As the Reynolds number increased, efficiency of the rotor also linearly increased. The experimental Reynolds number was 8.67×10^5, and the inflow wind speed was 14 m/s. The inflow wind speed was quite high, and the maximum efficiency was 24–25%. For the analysis model, flow analysis was conducted on the semi-circular type blades with endplates, with a rotor diameter of 1 m and height of 1 m, in the same manner as in the previous studies under the same Reynolds number conditions. Figure 3 shows the experimental data and simulation results. The compared power coefficient was calculated as Equation (1)

$$C_P = \frac{P_{rotor}}{P_{available}} = \frac{P_{rotor}}{\frac{1}{2}\rho A V^3}, \quad (1)$$

where ρ represents the density, and A is the product of the rotor diameter and height (D × H), which are equal to 0.9 m and 1 m, respectively. The rotor efficiency of the experimental data increased with the TSR, and maximum efficiency of more than 24% could be observed when the TSR value was approximately 0.9. In the simulation results, the rotor efficiency also increased with increasing TSR, and the maximum efficiency occured when the TSR value was approximately 0.8, which is similar to the tendency of the test data. The flow analysis and test data showed similar rotor efficiencies and the same maximum efficiency (24–25%) corresponding with the TSR change, thereby sufficiently validating the results obtained through numerical analysis.

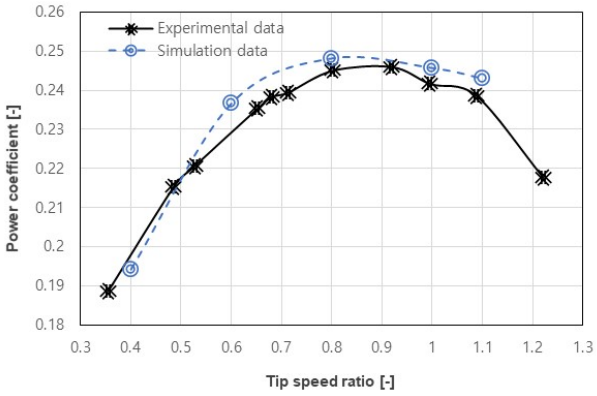

Figure 3. Test data comparison for examining the CFD analysis results.

3. Estimation of Rotor Power

The Savonius wind turbine rotates owing to lift and drag. In Figure 4, the Savonius wind turbine rotates clockwise because the torque developed by the concave blade in the wind direction is larger than that of the convex blade [23]. To improve the rotor performance, it is necessary to minimize the negative torque generated in the direction opposite to that of the rotor rotation. Because the blades in this study had to be composed of fabric materials, three types of blade geometries were considered based on manufacturability. The application of endplates may increase the rotor efficiency, but research was conducted without endplate application to decrease the manufacturing cost and improve safety. The semi-circular type blade, which is the basic geometry, can be classified under the Bach and elliptical types according to the blade curvature [24,25]. The common design parameters (AR and OR) of each Savonius blade were determined by conducting CFD analysis of the semi-circular type. Using the design parameters shown in Figure 4, the AR was defined

as the ratio of the blade height to its width (H/D) and the OR was defined as the ratio between the blade width and blade overlap length (e/d). Regarding the design parameters that determine the curvature of each blade, the values that led to the highest efficiency were determined through a case study, and the performance of each blade geometry was compared.

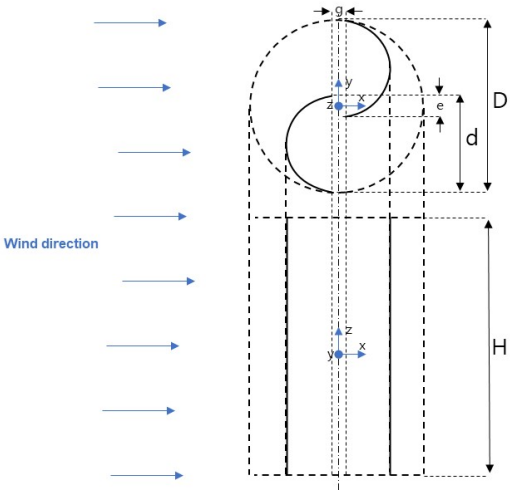

Figure 4. Savonius wind turbine geometry and design parameter definitions.

3.1. Design Paramaters

The efficiency of the Savonius rotor was highest when the AR was 2.4 and remained similar when the AR ranged from 2.4 to 3.3 [26]. For the initial analysis model in this study, the AR was determined to be 3.2 with D = 0.8 m and H = 1.28 m. The flow in the overlap area (e) improved the rotor performance by generating lift on the concave blade that receives the wind [27]. For the same rotor diameter, the blade length (d) varied depending on the OR. Ushiyama presented the highest rotor performance when the OR was 1/6 [16]. In this study, the rotor efficiencies for OR values zero (at d = 0.4 m) and 1/6 (at d = 0.43 m) were compared and maximum efficiencies of 12 and 16%, respectively, were observed, as shown in Figure 5a. Figure 5b presents the efficiencies of the two rotors, and a significant difference in performance depending on the OR can be observed. The OR was determined by examining the previous studies mentioned above. To determine the appropriate design values for the 100-W-class rotor targeted in this study, the power and efficiency corresponding to different H and D values were analyzed. The reference geometry was defined as RotorV3 in Table 1, and the rotor types were classified into four groups. For Group 1, D was fixed at 600 mm based on RotorV3 and H was varied. For Group 2, D and H were varied based on the swept area A of RotorV3 (A = 0.9 m^2). For Group 3, H was fixed at 1500 mm based on RotorV3 and D was varied. For Group 4, D and H were varied based on the swept area of RotorV3 (A = 0.9 m^2).

For the same TSR, the rotational speed increases as the AR of each geometry decreases, thereby resulting in an increase in efficiency. Therefore, flow analysis was conducted at a constant rotational speed (150 rpm) to compare the power and efficiency corresponding to different H and D values. Figure 6 shows the rotor power and efficiency for each case. As A increases, the power and efficiency increase correspondingly. When A is constant, the power and efficiency increase as the value of AR increases. However, in the case of RotorV5, RotorV6, and RotorV7, all of which had the same value of A, the rotor performance decreased under the condition of RotorV7, i.e., when AR was 2.8. This finding indicates that the most efficient design can be achieved when the AR value is maintained above 2.8. Among all the cases, RotorV10 exhibited the best design value considering the stable power generation at the targeted 100 W and structural stability.

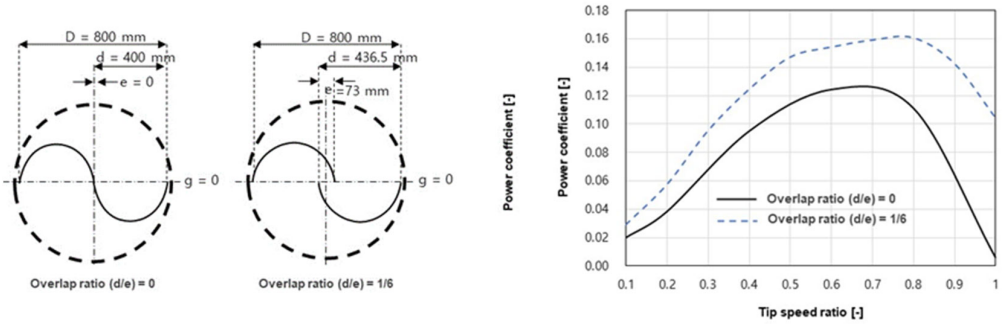

(**a**) (**b**)

Figure 5. Rotor efficiency changes according to the presence/absence of overlap: (**a**) Rotor geometry comparison, (**b**) Rotor power.

Table 1. Definitions of design parameters and analysis cases for a semi-circular rotor.

Rotor Type	D mm	H mm	d mm	A m^2	AR (H/D)	OR (e/d)
RotorV1	800	1280	436.5	1	3.2	0.167
RotorV2	600	1800	330	1.1	5.9	0.182
RotorV3	600	1500	330	0.9	5.0	0.182
RotorV4	600	1200	330	0.7	4.0	0.182
RotorV5	500	1800	275	0.9	7.1	0.182
RotorV6	600	1290	385	0.9	3.7	0.182
RotorV7	700	1125	440	0.9	2.8	0.182
RotorV8	500	1500	275	0.8	5.9	0.182
RotorV9	550	1500	303	0.8	5.6	0.182
RotorV10	650	1500	358	1	4.5	0.182
RotorV11	400	2450	220	0.9	11.1	0.182
RotorV12	450	2200	250	0.9	9.1	0.182
RotorV13	550	1840	300	0.9	5.9	0.182

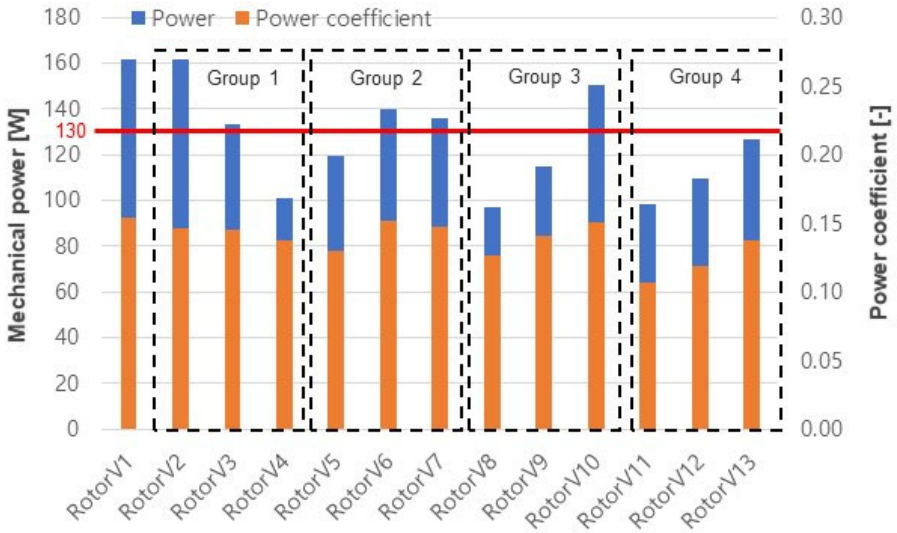

Figure 6. Rotor power and efficiency according to semi-circular rotor design parameters.

3.2. Comparison of Various Rotor Types

To compare the performance corresponding to the Savonius rotor geometry, semi-circular, Bach, and elliptical rotors were considered. The OR (0.182) and AR (4.5) values of RotorV10 determined by analyzing the design parameters of the semi-circular rotor were applied. In addition, d, H, and the width (W) of each configuration were modeled in the

same way as for RotorV10, which was a semi-circular rotor. In the case of the Bach type, g was set to 10% of the blade length because g = 0 causes the blades to overlap during the design process. For the elliptical type, the distance from the center of the ellipse to the end point (A) was set to be the same as d. The design specifications are shown in Figures 7 and 8, and Table 2 presents the power generated during one rotor rotation at 150 rpm. Although there was no significant difference in performance between the semi-circular and elliptical types owing to their similar geometries, the elliptical type exhibited better performance. Conversely, the Bach type displayed significant difference between maximum and minimum power and showed the worst performance with 11% efficiency. Because the design values of the Bach and elliptical types in Figure 7 were determined based on RotorV10, it was necessary to define the design parameters for the blade geometry and conduct additional analysis to maximize the performance of each rotor. Therefore, the AR and OR were applied in the same manner as for RotorV10, and design parameters for the blade geometry were re-defined to improve the performance of the Bach and elliptical types, as shown in Figure 9.

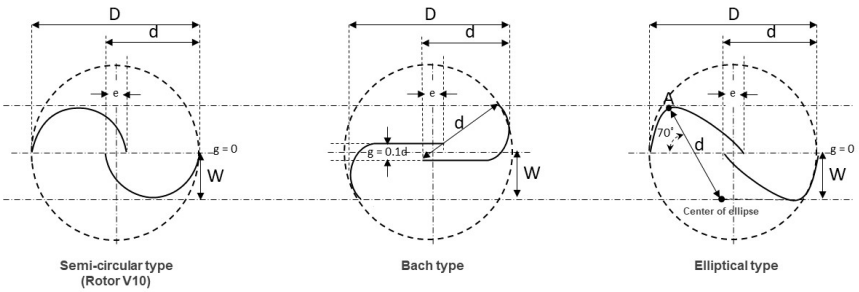

Figure 7. Bach and elliptical rotor design geometries according to semi-circular geometry.

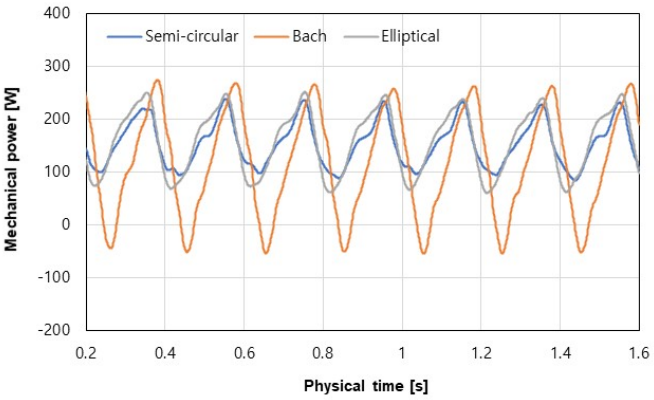

Figure 8. Rotor power according to rotor rotation position.

Table 2. Comparison of average rotor power and efficiency according to rotor geometry.

Type	Power [W]	Power Coefficient [–]
Semi-circular (Rotor V10)	151	0.15
Bach	114	0.11
Elliptical	155	0.16

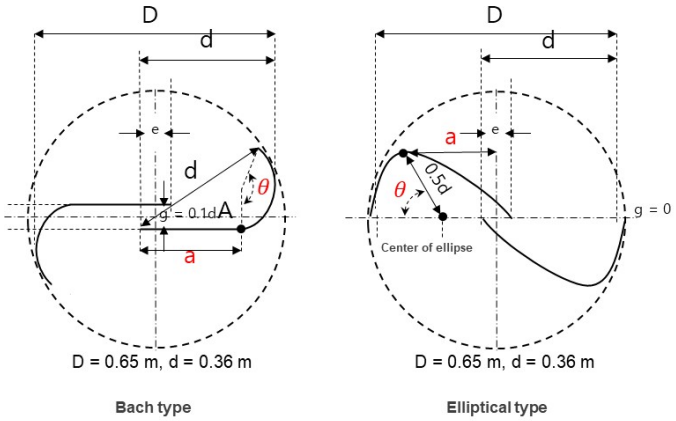

Figure 9. Definitions of design parameters for Bach and elliptical rotors.

Tables 3 and 4 summarize the performance and efficiency of the Bach and elliptical types, respectively, consequent to changes in the design parameters under conditions with TSR value of 0.6. In the case of the Bach type, the blade curvature increased as a decreased and negative torque did not occur when a < 0.22 m. As θ decreased, the blade curvature decreased, and the difference between the minimum and maximum torque increased. Among all the cases, the BachV5 (a = 0.3D, θ = 135°) geometry showed the lowest difference between the minimum and maximum power and the highest average power generation. In the case of the elliptical type, because the blade geometry is similar to that of the semi-circular type, with a decrease in a, both power and efficiency decreased as well. Conversely, the power and efficiency increased in correspondence with an increase of θ due to increase in the curvature of the rotor; however, the trend reversed when θ exceeded 40° at which point the performance declined. The maximum efficiency attained with the elliptical geometry was 18%, and the average power was the highest at a = 0.41D and θ = 40° (EllipticalV8).

To compare the performance of the three types of rotors, the rotor power in relation to the TSR at a wind speed of 12 m/s is shown in Figure 10. The semi-circular type exhibited lowest power when the TSR range was between 0.1 and 0.4, beyond which its power increased until TSR = 0.8; the power reduction rate was not high compared to those with other rotor geometries. For the Bach and elliptical types, the average power tended to decrease due to the significant difference between the minimum and maximum power. In particular, the maximum efficiency, which was attained when TSR > 0.6, and the power difference significantly increased depending on the rotor rotation position. Therefore, taking into consideration the ease of manufacture due to its simple design geometry and the stability in power generation capability, the semi-circular type was finally selected.

Table 3. Rotor power and efficiency according to Bach rotor design parameters.

Type	a m	θ °	Power (min) W	Power (max) W	Power W	Power Coefficient -
Bach V1	0.24	135	−16	324	151	0.15
Bach V2	0.23	135	−9	319	155	0.16
Bach V3	0.22	135	2	304	158	0.16
Bach V4	0.21	135	6	304	162	0.16
Bach V5	0.2	135	11	298	165	0.17
Bach V6	0.2	125	1	296	167	0.17
Bach V7	0.2	130	8	300	167	0.17
Bach V8	0.2	140	14	302	163	0.16
Bach V9	0.2	145	4	314	159	0.16
Bach V10	0.2	150	−14	311	155	0.15

Table 4. Rotor power and efficiency according to elliptical rotor design parameters.

Type	a m	θ °	Power (min) W	Power (max) W	Power W	Power Coefficient -
EllipticalV1	0.29	45	15	308	164	0.16
EllipticalV2	0.28	45	22	307	173	0.17
EllipticalV3	0.27	45	17	310	181	0.18
EllipticalV4	0.26	45	22	309	180	0.18
EllipticalV5	0.25	45	25	309	181	0.18
EllipticalV6	0.27	30	−5	304	175	0.18
EllipticalV7	0.27	35	14	311	181	0.18
EllipticalV8	0.27	40	19	315	183	0.18
EllipticalV9	0.27	50	23	313	175	0.18
EllipticalV10	0.270	55	32	313	170	0.17

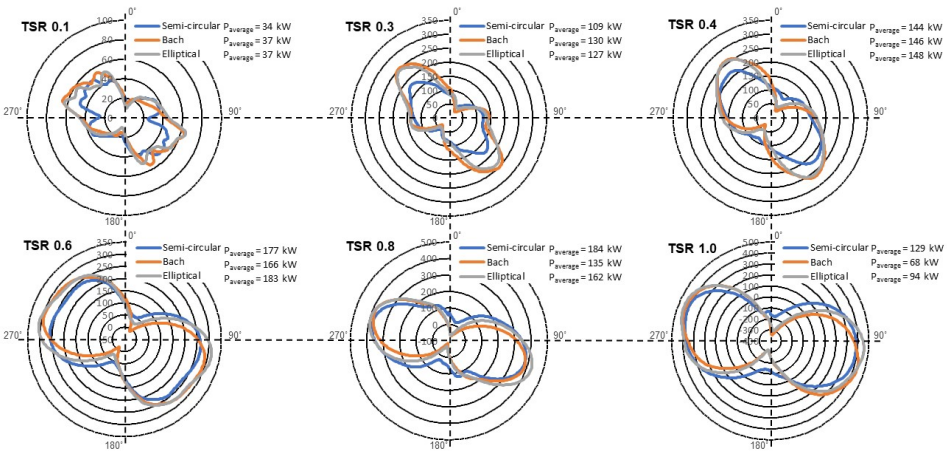

Figure 10. Comparison of rotor power during one rotation according to TSR.

4. Effect of Rotor Arrangement

Wind turbines produce electrical energy by converting wind energy into kinetic energy. A wind turbine that is positioned in the wake of another wind turbine shows performance degradation because it is affected by the wind turbine in front. Hence, when small wind turbines are used, they must be arranged within the minimum available space so as to maximize efficiency and energy generation. Vertical axis wind turbines have a structure in which the torque significantly varies depending on the rotor position during rotation. Therefore, the wake flow, which changes during rotor rotation, was analyzed in a single rotor simulation, and the changes in rotor performance under various rotor arrangements were also analyzed.

4.1. Analysis of Single Rotor Wake

To analyze the changes in the wind flow that passes through a rotor, the velocity and pressure according to the rotation position of a single rotor were analyzed. Figures 11 and 12 present the pressure and velocity flow fields, respectively, of a rotor rotating in the counterclockwise direction at 30° intervals. The inflow wind direction was the positive x-direction in all cases. Because the positions of blades 1 and 2 were symmetrical in 180° intervals, the rotation angle was expressed from 30 to 180°. As Figure 11 shows, when the rotor rotated by 30° counterclockwise, an area of high pressure was evident on the convex surface of blade 1 and an area of relatively low pressure occurred on the concave surface. In this instance, a torque in the direction opposite to the rotation direction occurred due to pressure difference between the convex and concave surfaces, and a thrust acting on the convex surface of blade 1 inhibited the rotor rotation. In addition, the separation of the vortex with low pressure at the tip of blade 2 reduced the pressure difference, resulting in low power

generation of 44 W. When the rotor was rotated by 60°, the pressure difference between the convex and concave surfaces of blade 1 was similar to that under the 30° rotor rotation condition, but the low-pressure area on the convex surface increased. In addition, because the thrust acting on the convex surface of blade 1 in the wind direction decreased due to the change in rotation position, the power generation increased. Thus, the highest power generation was observed at 60–120°, when the torque acting in the direction opposite to the thrust acting on blade 1 decreased. In the velocity flow field behind the rotor in Figure 12, areas in which the velocity decreased and increased due to the rotating blade can be seen. The area in which the velocity decreased remained relatively constant as the rotor rotation position changed. Under the 30° and 180° conditions with low rotor power, however, a vortex with high velocity occurred at the tip of blade 2, and it expanded as it moved backward. Therefore, the performance of the Savonius turbine was improved when the torque and thrust acting in the direction opposite to the rotation direction were minimized as mentioned above. In the case of a downstream turbine, a rotor arrangement that can locate the rotation-inhibiting blade in the low-velocity zone and torque generation by the blade in the rotation direction in the high-velocity zone are required.

4.2. Multi Turbine Interaction Effect

To examine the influence of spacing between rotors, the power generation in relation to the separation distance between rotors 1 and 2 in the x-direction was calculated, as shown in Figure 13a. Figure 13b depicts the power according to the rotor rotation position, and it is evident that the power generation of rotor 2 decreased as it approached rotor 1. The wake zone of rotor 1 in the x-direction had low velocity, as depicted in Figure 12. Consequently, the power decreased by more than 68% (Rotor 2_3.5D) despite an increase in the separation distance between the turbines. To minimize the power reduction of the rotor located in the wake zone, the performance corresponding to the separation distances in the x- and y-directions was analyzed. Table 5 summarizes the various arrangements and analysis results. For cases 1–3, the separation distance in the x-direction was fixed at 2D and the separation distance in the y-direction was varied. For cases 4–6, the separation distance in the x-direction was fixed at 3D and the separation distance in the y-direction was varied. Based on the results for cases 1 and 4 in which rotor 2 was 1D away from rotor 1 in the y-direction, it can be observed that the power decreased owing to the interference between the front and rear turbines. Moreover, the performance of rotor 2 in case 4 is lower than that in case 1, even though it is 3D away from rotor 1 in the x-direction. For a more detailed analysis, the velocity distribution of each case is shown in Figure 14. The results for cases 1 and 4 in Figure 14 indicate that the power generation of rotor 2 decreased because wind with low velocity was introduced to the rotor 2, which received wind in the rotation direction due to the wake of rotor 1 in the front. Between cases 2 and 5, case 2 generated higher power than case 5 because the vortex with high velocity generated by rotor 1 acted on rotor 2 before it got diffused. Between cases 3 and 6, the power generation of case 3 was higher. It is noteworthy that cases 3 and 6 generated higher power than cases 2 and 5 because rotor 2 was not influenced by the wake produced by rotor 1 due to further movement in the y-direction. The above results confirm that the performances of the turbines were not influenced by each other when rotor 2 was 2D away from rotor 1 in the x- or y-direction, or when the rotors were arranged in the positive y-direction with respect to rotor 1.

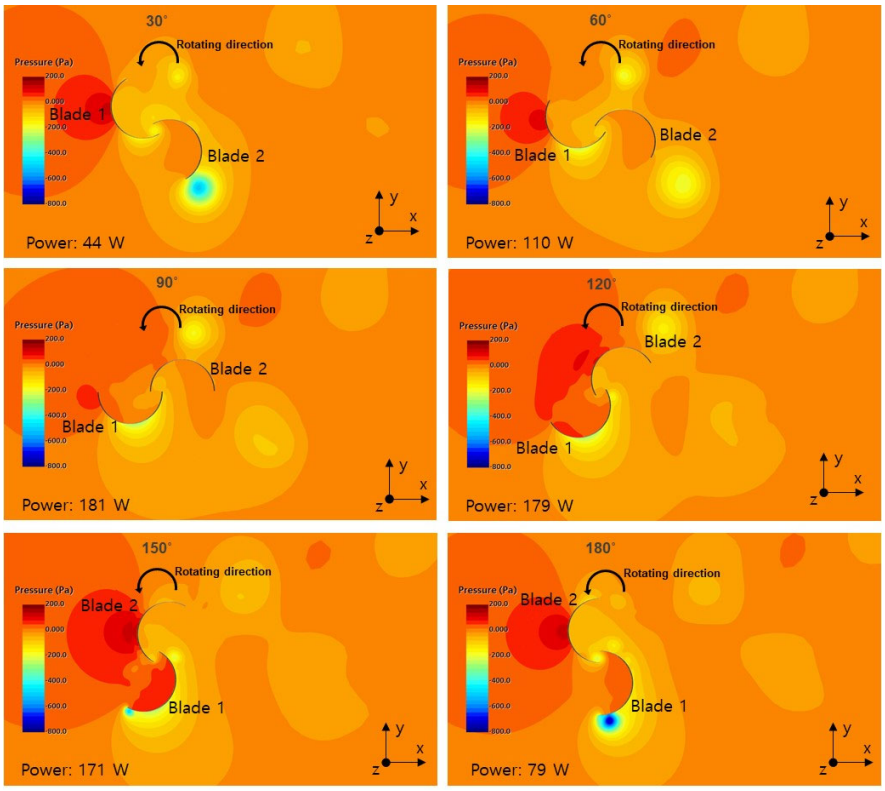

Figure 11. Pressure distribution according to rotor rotation position.

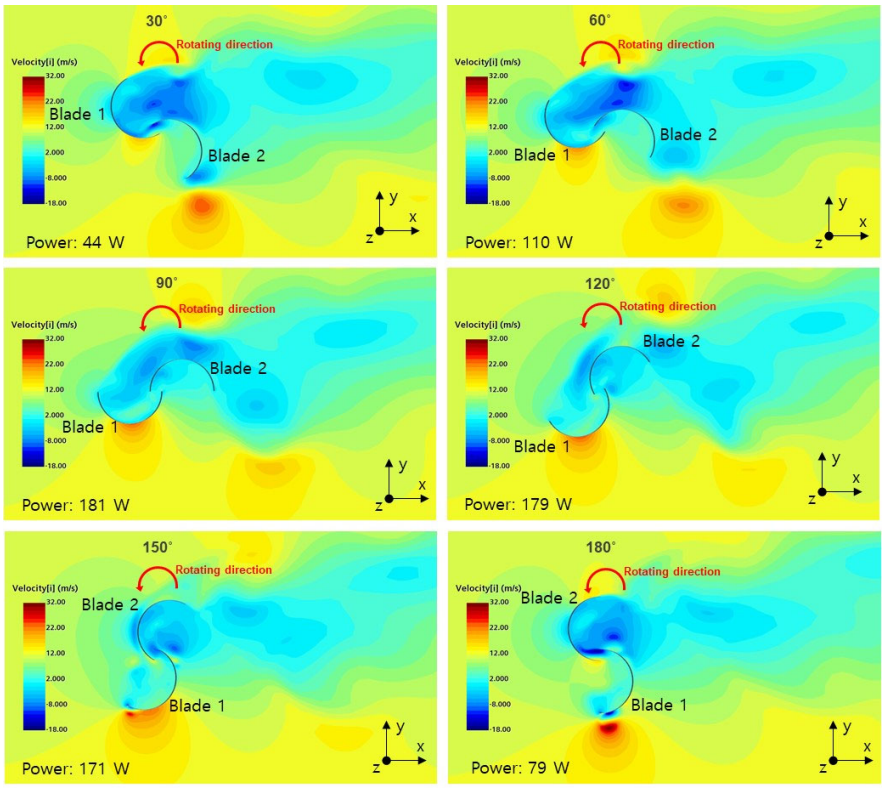

Figure 12. Velocity distribution according to rotor rotation position.

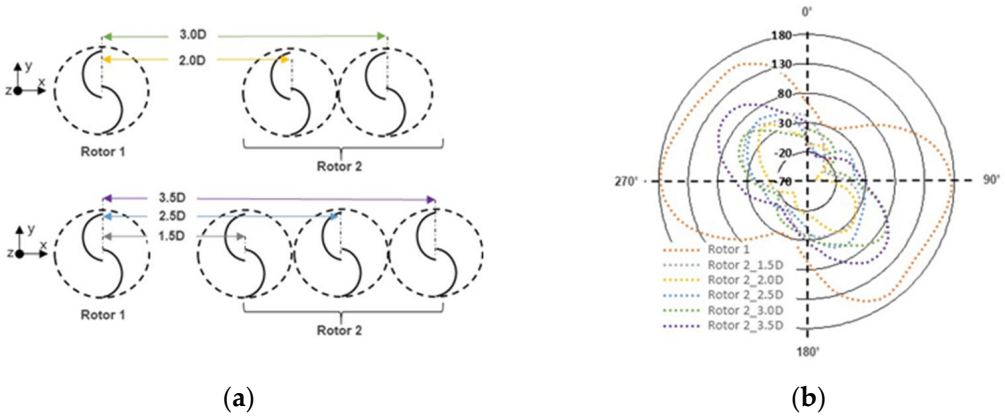

(**a**) (**b**)

Figure 13. Analysis conditions for rotor spacing examination and comparison of power per rotor rotation: (**a**) Rotor arrangement cases, (**b**) Power per rotor rotation.

Table 5. Rotor power according to downstream rotor position.

Case Number	Rotor 2 Position x Axis	Rotor 2 Position y Axis	Power Rotor 1 [W]	Power Rotor 2 [W]	Rotor 2 Power Reduction Rate [%]
Case 1	2D	1D	121.9	82.2	−32.6
Case 2	2D	1.5D	124.9	128.7	3
Case 3	2D	2D	124.8	132.2	5.9
Case 4	3D	1D	121.9	55.8	−54.3
Case 5	3D	1.5D	123.5	99	−19.9
Case 6	3D	2D	124.5	117.1	−6

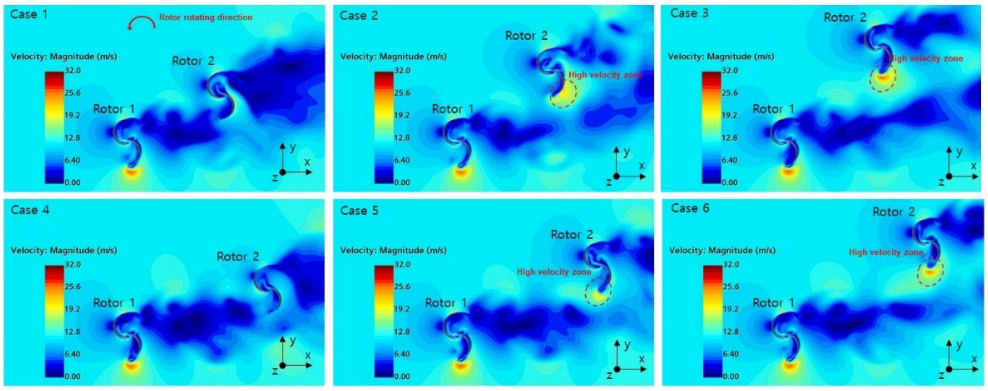

Figure 14. Velocity distribution according to downstream rotor position.

To examine more diverse arrangement conditions, an analysis was conducted considering three rotors. Table 6 summarizes the arrangement cases for the three rotors and the power of each rotor, and Figure 15 shows the conditions of case 1. Because rotors 1 and 3 were set to rotate clockwise, rotor 2 was set to rotate counterclockwise so as to utilize the vortex with increased wind speed generated by rotor 1. When the separation distance of other rotors from rotor 1 in the x-direction increased from 2D to 3D, the power generation of rotors 2 and 3 decreased. Further, when the separation distance between rotors 1 and 3 in the y-direction increased to 1.5D and 2.0D, the power of rotor 3 increased. When the combined power generation of all the three rotors are considered together, it was evident that case 9 generated the maximum power. The distances of rotors 2 and 3 from rotor 1 were 2D in both the x-axis and y-axis directions in case 9, and the results were identical to those obtained earlier through analysis when two rotors were taken into consideration. In case 9, the rotor 1, rotor 2, and rotor 3 attained efficiencies of 17, 19, and 18%, respectively. The reduction in the efficiency of rotor 1 could be attributed to the fact that rotors 2 and

3 utilized the kinetic energy boost that was caused by the wake of rotor 1. The optimal positions of the downstream turbines need to be examined to use the high-speed vortex generated periodically by the upstream turbine. The power generation of rotor 1 in Table 6 showed that the downstream rotors influenced the performance of the upstream rotor. Figure 16 presents the velocity distribution according to the rotor rotation position in case 9. The wake zone of rotor 1 can be divided into high- and low-velocity zones, and it can be seen that rotors 2 and 3 were not located in the low-velocity zone. Consequently, case 9 was the optimal arrangement that can minimize the loss by the downstream rotors because it demonstrates the highest power generation of rotor 1 among all the cases.

Table 6. Arrangement cases for three rotors and power of each rotor.

Case Number	Rotor 2 Position		Rotor 3 Position		Power Rotor [W]	Power Rotor 2 [W]	Power Rotor 3 [W]	Power sum [W]
	x Axis	y Axis	x Axis	y Axis				
Case 1	3.0 D	2.0 D	2.0 D	1.0 D	121.6	119.8	124.7	366.1
Case 2	3.0 D	2.0 D	2.0 D	1.5 D	125.4	119	129.5	373.8
Case 3	3.0 D	2.0 D	2.0 D	2.0 D	126.4	118.9	131	376.3
Case 4	3.0 D	2.0 D	3.0 D	1.0 D	121.3	120.4	130.7	372.5
Case 5	3.0 D	2.0 D	3.0 D	1.5 D	123.6	119.6	131.2	374.4
Case 6	3.0 D	2.0 D	3.0 D	2.0 D	123.7	121	129.8	374.5
Case 7	2,0 D	2.0 D	2.0 D	1.0 D	121.7	139.8	127.3	388.8
Case 8	2.0 D	2.0 D	2.0 D	1.5 D	125.5	136.4	131.6	393.5
Case 9	2.0 D	2.0 D	2.0 D	2.0 D	128.4	140.1	129.7	398.1
Case 10	2.0 D	2.0 D	3.0 D	1.0 D	122.8	137.3	126	386
Case 11	2.0 D	2.0 D	3.0 D	1.5 D	125	137.3	127.4	389.7
Case 12	2.0 D	2.0 D	3.0 D	2.0 D	126.8	137	127	390.8

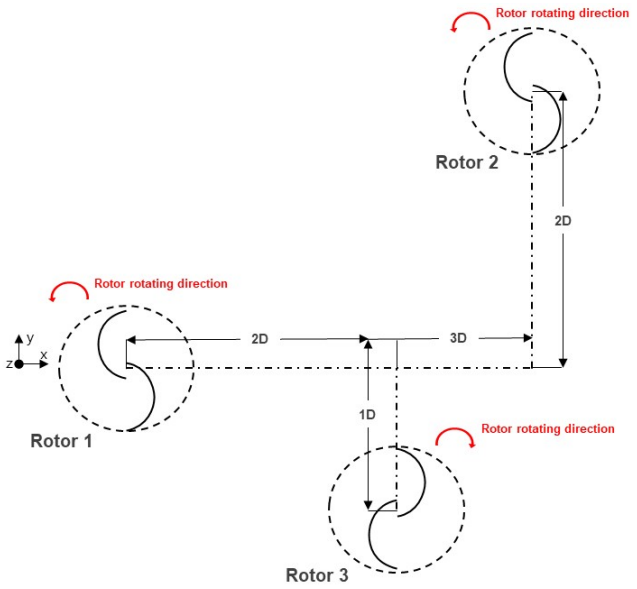

Figure 15. Arrangement spacing and rotation directions of three rotors in case 1.

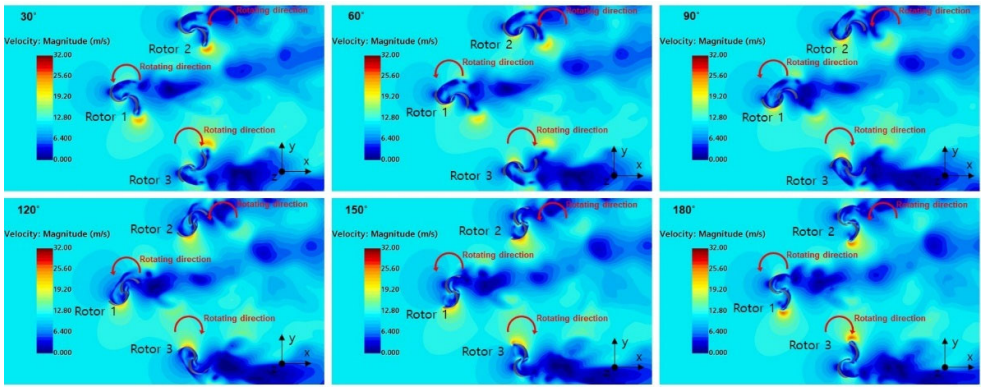

Figure 16. Velocity distribution according to rotor rotation position for three rotors in case 9.

5. Conclusions

This paper presents a conceptual design and modeling method for the development of small urban wind turbines as well as a wake flow analysis of the rotor arrangement that can maximize rotor efficiency. A three-dimensional CFD simulation was performed, and the analysis results were compared with the experimental data from previous studies to examine their validity. At a Reynolds number of 8.67×10^5 (wind speed 14 m/s), the experimental data and CFD analysis results showed similar efficiency (up to 24%). Because the objectives of this study were to ensure stability in unexpected situations and to develop an eco-friendly turbine using recycled fabric materials, additional devices and endplates that could improve the rotor efficiency were not applied. The OR and AR, which are the design parameters that most significantly affect rotor performance, were determined based on a semi-circular rotor. The performance was compared when the OR was 0 and 1/6, and higher efficiency was confirmed when the OR was 1/6. Thirteen cases were generated according to the AR, and the power change was compared. Efficiency was realized when the AR was designed to be above 2.8, and the targeted power was achieved by RotorV10, which had an AR of 4.5. The performance of the Bach and elliptical types was analyzed to determine a geometry that could improve the rotor performance. The OR and AR identified based on RotorV10 were applied, and the performance of the Bach and elliptical types according to the design parameters was analyzed. In addition, the power generated by each type of rotor was compared. The three geometries exhibited similar maximum efficiencies (17–18%), but the difference between the maximum and minimum power generated was found to be large for the Bach and elliptical types. Therefore, the semi-circular type, which is capable of stable power generation, was finally selected. The optimal rotor arrangement was examined by arranging two and three rotors through wake flow analysis for a single rotor. The Savonius turbine has a structure in which the torque significantly varies depending on the rotor position during rotation. For the blades of a downstream turbine, a rotor arrangement that can locate the blade generating negative torque in the low-velocity zone and the blade generating positive torque in the high-velocity zone was required. Considering two rotors, the efficiency did not decrease when the separation distance between the upstream and downstream rotors was 2D in both the x- and y-directions. For three rotors, the efficiency again did not decrease when the separation distance between the upstream and downstream rotors was 2D in both the x- and y-directions.

The aforementioned results confirm that a semi-circular rotor, which has a small difference between the maximum and minimum power generated, enables stable power generation despite a slight reduction in efficiency. The installation of multiple turbines does not decrease the performance, and the power can be improved by placing the downstream turbines at a distance corresponding to twice the rotor diameter from the upstream turbine. However, as this study has been conducted under the assumption of a steady inflow of wind in one direction, the positions of the downstream turbines with respect to the upstream turbine may require to be changed when the actual wind direction changes.

Therefore, research on the construction of a cluster that enables yaw motion with respect to the upstream turbine is required to develop a small wind turbine system that is stable and does not experience reduced turbine efficiency.

Author Contributions: Conceptualization, methodology, software, validation, formal analysis, investigation, writing—original draft preparation, visualization, H.I.; Conceptualization, formal analysis, writing (review and editing), supervision, resources, B.K. All authors have read and agreed to the published version of the manuscript.

Funding: This work was supported by the Korea Institute of Energy Technology Evaluation and Planning (KETEP) and the Ministry of Trade, Industry & Energy (MOTIE) of the Republic of Korea (No. 20203030020370).

Data Availability Statement: Not applicable.

Conflicts of Interest: The authors declare that they have no conflict of interest.

References

1. GWEC. Global Wind Energy Council, Global wind report 2021. GWEA: Brussels, Belgium. Available online: https://gwec.net/wp-content/uploads/2021/03/GWEC-Global-Wind-Report-2021.pdf (accessed on 11 December 2022).
2. Akwa, J.V.; Vielmo, H.A.; Petry, A.P. A review on the performance of Savonius wind turbines. *Renew. Sustain. Energy Rev.* **2012**, *16*, 3054–3064. [CrossRef]
3. Savonius, S. The s-rotor and its applications. *Mech. Eng.* **1931**, *53*, 333–338.
4. Saad, A.S.; Elwardany, A.; El-Sharkawy, I.I.; Ookawara, S.; Ahmed, M. Performance evaluation of a novel vertical axis wind turbine using twisted blades in multi-stage Savonius rotors. *Energy Convers. Manag.* **2021**, *235*, 114013. [CrossRef]
5. Shikha; Bhatti,, T.S.; Kothari, D.P. Wind energy conversion systems as a distributed source of generation. *J. Energy Eng.* **2003**, *129*, 69–80.
6. Mohamed, M.H.; Janiga, G.; Pap, E.; Thévenin, D. Optimal blade shape of a modified Savonius turbine using an obstacle shielding the returning blade. *Energy Convers. Manag.* **2011**, *52*, 236–242. [CrossRef]
7. Roy, S.; Mukherjee, P.; Saha, U.K. Aerodynamic Performance Evaluation of a Novel Savonius-Style Wind Turbine Under an Oriented Jet. In Proceedings of the Gas Turbine India Conference, New Delhi, India, 15–17 December 2014. V001T08A001.
8. Altan, B.D.; Atilgan, M. The use of a curtain design to increase the performance level of a Savonius wind rotors. *Renew. Energy* **2010**, *35*, 821–829. [CrossRef]
9. Abraham, J.P.; Plourde, B.D.; Mowry, G.S.; Minkowycz, W.J.; Sparrow, E.M. Summary of Savonius wind turbine development and future applications for small-scale power generation. *J. Renew. Sustain. Energy.* **2012**, *4*, 042703. [CrossRef]
10. El-Askary, W.A.; Nasef, M.H.; AbdEL-hamid, A.A.; Gad, H.E. Harvesting wind energy for improving performance of Savonius rotor. *J. Wind Eng. Ind. Aerodyn.* **2015**, *139*, 8–15. [CrossRef]
11. Rahai, H.R.; Hefazi, H. Development of optimum design configuration and performance for vertical axis wind turbine. In *Feasibility Analysis and Final EISG Report*; California Energy Commission: Sacramento, CA, USA, 2005; CEC-500-2005-084.
12. Al-Kayiem, H.H.; Bhayo, B.A.; Assadi, M. Comparative critique on the design parameters and their effect on the performance of s-rotors. *Renew. Energy* **2016**, *99*, 1306–1317. [CrossRef]
13. Roy, S.; Saha, U.K. Review of experimental investigations into the design, performance and optimization of the Savonius rotor. *Proc. Inst. Mech. Eng. A* **2013**, *227*, 528–542. [CrossRef]
14. Fujisawa, N. On the torque mechanism of Savonius rotors. *J. Wind Eng. Ind. Aerodyn.* **1992**, *40*, 277–292. [CrossRef]
15. Blackwell, B.F.; Sheldahl, R.E.; Feltz, L.V. *Wind Tunnel Performance Data for Two and Three-Bucket Savonius Rotors*; Government Report; Journal of Energy: Albuquerque, NM, USA, 1977.
16. Ushiyama, I.; Nagai, H. Optimum design configurations and performance of Savonius rotors. *Wind Eng.* **1988**, *12*, 59–75.
17. Akwa, J.V.; Da Silva, G.A., Jr.; Petry, A.P. Discussion on the verification of the overlap ratio influence on performance coefficients of a Savonius wind rotor using computational fluid dynamics. *Renew. Energy* **2012**, *38*, 141–149. [CrossRef]
18. Gupta, R.; Das, R.; Sharma, K.K. Experimental Study of a Savonius-Darrieus Wind Machine. In *Proceedings of the International Conference on Renewable Energy for Developing Countries*; University of Columbia: Washington, DC, USA, 2006.
19. Roy, S.; Saha, U.K. Numerical Investigation to Assess an Optimal Blade Profile for the Drag Based Vertical Axis Wind Turbine. In *ASME International Mechanical Engineering Congress and Exposition*; American Society of Mechanical Engineers: San Diego, CA, USA, 2013; V06AT07A084.
20. Banerjee, A.; Roy, S.; Mukherjee, P.; Saha, U.K. Unsteady Flow Analysis Around an Elliptic-Bladed Savonius-Style Wind Turbine. In *Gas Turbine India Conference*; American Society of Mechanical Engineers: New York, NY, USA, 2014; V001T05A001.
21. Alon, N.; Saha, U.K. Influence of blade profiles on Savonius rotor performance: Numerical simulation and experimental validation. *Energy Convers. Manag.* **2019**, *186*, 267–277. [CrossRef]
22. Zhang, B.; Song, B.; Mao, Z.; Tian, W. A novel wake energy reuse method to optimize the layout for Savonius-type vertical axis wind turbines. *Energy* **2017**, *121*, 341–355. [CrossRef]

23. Kacprzak, K.; Liskiewicz, G.; Sobczak, K. Numerical investigation of conventional and modified Savonius wind turbines. *Renew. Energy* **2013**, *60*, 578–585. [CrossRef]
24. Roy, S.; Saha, U.K. Wind tunnel experiments of a newly developed two-bladed Savonius-style wind turbine. *Appl. Energy* **2015**, *137*, 117–125. [CrossRef]
25. Meri Ar, S.; Bin Salleh, H. Numerical investigation of Savonius rotor elliptical and the design modification on a blade shape. In *Advances in Material Sciences and Engineering*; Springer: Singapore, 2020; pp. 177–185.
26. Le Gourieres, D. *Wind Power Plants: Theory and Design*; Elsevier: Amsterdam, The Netherlands, 2014.
27. Shaheen, M.; El-Sayed, M.; Abdallah, S. Numerical study of two-bucket Savonius wind turbine cluster. *J. Wing Eng. Ind. Aerodyn.* **2015**, *137*, 78–89. [CrossRef]